Study of the reaction $\bar{p}p \to \phi\phi$ from 1.1 to 2.0 GeV/c

C. Evangelista and A. Palano
University of Bari and INFN, I-70126 Bari, Italy

D. Drijard, N. H. Hamann,* R. T. Jones,† B. Mouëllic, S. Ohlsson, and J.-M. Perreau
CERN, CH-1211 Geneva, Switzerland

W. Eyrich, M. Moosburger, S. Pomp, and F. Stinzing
University of Erlangen-Nürnberg, W-8520 Erlangen, Germany

H. Fischer, J. Franz, E. Rössle, H. Schmitt, and H. Wirth‡
University of Freiburg, W-7800 Freiburg, Germany

A. Buzzo, K. Kirsebom, M. Lo Vetere, M. Macrì, M. Marinelli, S. Passaggio, M. G. Pia, A. Pozzo, E. Robutti, and A. Santroni
University of Genova and INFN, I-16132 Genova, Italy

P. T. Debevec, R. A. Eisenstein,§ P. G. Harris,‖ D. W. Hertzog, S. A. Hughes, P. E. Reimer,¶ and J. Ritter
University of Illinois, Urbana, Illinois 61801

R. Geyer, K. Kilian, W. Oelert, K. Röhrich,‡ M. Rook, and O. Steinkamp
Institut für Kernphysik, Forschungszentrum Jülich, D-5170 Jülich, Germany

H. Korsmo and B. Stugu**
University of Oslo, N-0316 Oslo, Norway

T. Johansson
Uppsala University, S-75121 Uppsala, Sweden
(Received 13 January 1998; published 7 April 1998)

A study has been performed of the reaction $\bar{p}p \to 4K^{\pm}$ using in-flight antiprotons from 1.1 to 2.0 GeV/c incident momentum interacting with a hydrogen jet target. The reaction is dominated by the production of a pair of ϕ mesons. The $\bar{p}p \to \phi\phi$ cross section rises sharply above threshold and then falls continuously as a function of increasing antiproton momentum. The overall magnitude of the cross section exceeds expectations from a simple application of the Okubo-Zweig-Iizuka rule by two orders of magnitude. In a fine scan around the $\xi/f_J(2230)$ resonance, no structure is observed. A limit is set for the double branching ratio $\mathrm{B}(\xi \to \bar{p}p) \times \mathrm{B}(\xi \to \phi\phi) < 6 \times 10^{-5}$ for a spin 2 resonance of M=2.235 GeV and $\Gamma = 15$ MeV. [S0556-2821(98)02511-9]

PACS number(s): 14.40.−n, 13.75.−n, 25.43.+t

I. INTRODUCTION

Beyond the common families of baryonic (qqq) and mesonic $(q\bar{q})$ states, glueballs $(gg$ or $ggg)$, hybrids $(q\bar{q}g)$ and multi-quark systems (e.g., $q\bar{q}q\bar{q}$) are predicted to exist based on the current understanding of QCD and QCD-inspired phenomenological models of hadrons. The question of the existence of these unusual hadronic bound systems is fundamental and should lead to a broader understanding of the behavior of QCD in the non-perturbative region. The experiment described below investigates the existence of gluonic hadrons in the mass range between 2.1 and 2.4 GeV/c^2. The technique requires a state, if found, to couple appreciably to both antiproton-proton (the entrance channel) and $\phi\phi$ (the exit channel). The parameter space explored is of particular interest in a search for the tensor glueball.

Gluonic hadrons are expected to populate the low mass region of the hadron spectrum together with normal $q\bar{q}$ states. Recent lattice QCD calculations locate the scalar $(J^{PC}=0^{++})$ glueball mass in the range of 1.5 to 1.7 GeV [1]. The tensor $(J^{PC}=2^{++})$ is the next low-lying glueball and is found to be approximately 1.5 times more massive than the scalar, thus it is postulated that it might be in the region explored by this experiment.

*Deceased.
†Present address: University of Connecticut, Storrs, CT.
‡Present address: Creative Services, St. Genis, France.
§Now at National Science Foundation, Washington, D.C.
‖Present address: University of Sussex, Falmer, Brighton, UK.
¶Present address: Los Alamos National Laboratory, Los Alamos, NM 87545.
**Present address: University of Bergen, Norway.

Several experimental approaches have been used to search for glueballs. The common theme is to choose a process, where a kinematical or dynamical filter strongly reduces the large production of standard $q\bar{q}$ mesons. Reactions intensively explored are peripheral hadron interactions [2], J/ψ radiative decays [3], central production [4], $\gamma\gamma$ collisions [5] and $\bar{p}p$ annihilations [6].

The study of the $\bar{p}p \to \phi\phi$ reaction is motivated by the expectation that, with essentially no common valence quarks between the initial and final states, the reaction is forbidden in first order. Indeed, a strict application of the empirical Okubo-Zweig-Iizuka (OZI) rule [7] suggests a cross section for $\bar{p}p \to \phi\phi$ of approximately 10 nb. In a previous publication [8], we reported the cross section at 1.4 GeV/c incident antiproton momentum to be 3.7 ± 0.8 μb and thus two orders of magnitude greater than estimated. The large $\bar{p}p \to \phi\phi$ cross section has been interpreted as coming from two-step processes [9,10], from intermediate glue [11], and/or from the intrinsic strangeness in the nucleons [12].

Here we review the appropriateness of the energy range of our study with respect to the possibility of exciting a gluonic resonance. As evidence, consider the current picture of candidate glueball states. The $f_0(1500)$, discovered by the Crystal Barrel experiment at the CERN Low-Energy Antiproton Ring (LEAR), has a width of $\Gamma \approx 120$ MeV and has been observed to decay to $\pi^0\pi^0$, $\eta\eta$ [13], $\eta\eta'$ [14] and $K\bar{K}$ [15] following $\bar{p}p$ annihilation at rest. The existence of this state has been confirmed in in-flight $\bar{p}p$ annihilations by experiment E760 at Fermilab [16]. It has been interpreted as the leading scalar glueball candidate. Alternate explanations feature strong gluonic content; the state could be a mixture of a glueball and nearby ordinary $q\bar{q}$ systems [17]. If identified with the scalar glueball, the implication from the lattice calculations is that the tensor mass should be in the 2.1 to 2.4 GeV range, where candidate glueball states have already been identified. These states include the $\xi/f_J(2230)$ which is observed in radiative J/ψ decays to $K\bar{K}$ [18] and also in decays to $\pi\pi$ and $p\bar{p}$ [19]. The width of this state ($\Gamma \approx 30 \pm 20$ MeV) is unexpectedly small, and has stimulated considerable interest. The spin-parity is undetermined, but is limited to $(\text{even})^+$. This channel is of interest to the present experiment since it couples to $\bar{p}p$. In another study [20] from this experiment, stringent limits were established on the double branching ratio $\mathrm{B}(\xi \to \bar{p}p) \times \mathrm{B}(\xi \to K_S^0 K_S^0)$ for the case of a narrow (i.e., $\Gamma < 30$ MeV) state.

Resonances in the $\phi\phi$ system have been observed in $J/\psi \to \gamma\phi\phi$ by Mark III and DM2. Each group saw a wide bump above $\phi\phi$ threshold peaking near 2.2 GeV and having a width of approximately 100 MeV. The preferred J^P assignment is 0^-, however, 2^+ contributions cannot be excluded [21].

The $\phi\phi$ system has been studied in exclusive $\pi^- p$ [22,23] and inclusive π^-Be induced interactions [24]. This reaction is expected to be highly suppressed based on the above OZI argument related to disconnected quark-line diagrams. However the suppression is not observed near threshold, a fact which could be explained by the production of intermediate gluonic resonances [11]. A partial wave analysis (PWA) of the exclusive data revealed the presence of three interfering $J^{PC} = 2^{++}$ resonances, the $f_2(2010)$, $f_2(2300)$ and $f_2(2340)$, originally called g_T states. The inclusive data show evidence for two structures with parameters compatible with those measured for the g_T states, but a PWA was not possible.

We report below on the evaluation of 58 independent measurements of the reaction $\bar{p}p \to 4K^{\pm}$ from which we determine the cross sections for $\bar{p}p \to \phi\phi$, $\bar{p}p \to \phi K^+ K^-$ and $\bar{p}p \to 4K^{\pm}$. A threshold enhancement is evident in the $\phi\phi$ cross section data. In the narrow region around the $\xi/f_J(2230)$ resonance, 17 measurements of the $\phi\phi$ cross section are reported in narrow energy steps covering a range of 45 MeV. Limits are set on the non-observation of this state.

II. THE EXPERIMENT

The JETSET (PS202) [25] experiment is designed to measure the reaction

$$\bar{p}p \to \phi\phi \to K^+K^-K^+K^- \tag{1}$$

as a function of incident antiproton momentum from 1.1 GeV/c to the highest momenta available at LEAR (2.0 GeV/c). The experiment makes use of the LEAR antiproton beam incident on an internal target provided by a hydrogen-cluster jet system. To obtain a measure of the absolute (and relative) luminosity at different antiproton momenta, $\bar{p}p$ elastic scattering events were recorded in parallel using a special dedicated trigger.

One key feature of reaction (1) in the energy range covered by this experiment is the fact that the outgoing kaons are constrained to a forward cone below 60°. Dominant in $\bar{p}p$ annihilation are the production of charged and neutral pions. These unwanted background reactions produce relatively fast charged particles and photons spread over a much larger angular range. The design of the detector and electronic trigger takes advantage of these facts by providing good charged-particle tracking and particle identification (PID) for forward angles, fast charged-particle multiplicity for triggering, and a large-acceptance photon rejection system. The philosophy followed to record and identify $4K^{\pm}$ events is to trigger only on the proper multiplicity pattern. In the offline analysis, events are required to have four well-determined tracks in the right kinematical range. Finally, these tracks are associated with hits in the PID detectors to determine compatibility with identification as kaons from the $4K$ final state.

A schematic view of the apparatus is shown in Fig. 1. Its basic structure is a hydrogen-cluster jet target (not shown) [26] with a density $\rho = 4 \times 10^{12}$ atoms/cm^2, surrounded by a compact detector. The jet is oriented horizontally and intersects the circulating antiproton beam at right angles. Around the interaction volume the LEAR ring is equipped with an oval vacuum chamber (0.03 radiation lengths thick) having horizontal and vertical half-axes of 78 and 38 mm, respectively. This limits the geometrical acceptance of the detector to polar angles $\theta_{lab} > 7°$, with complete coverage of azimuthal angles only for $\theta_{lab} > 15°$.

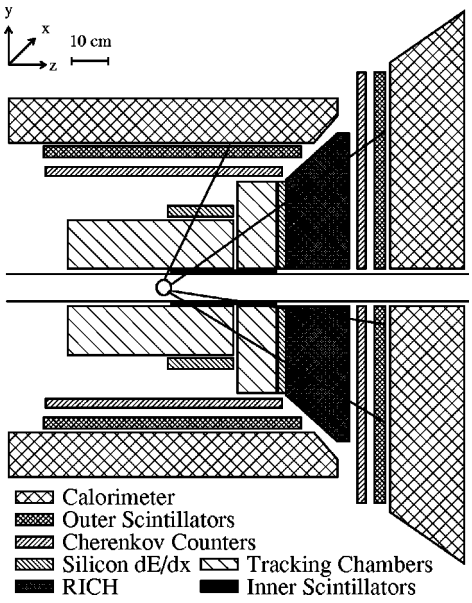

FIG. 1. Layout of the JETSET/PS202 experiment, showing the major detector components. A typical event with three forward and one barrel track is shown.

The overall structure of the detector includes a ''forward'' and a ''barrel'' sector with polar angular coverage from 7°–45° and 45°–135°, respectively. Immediately outside of the beam pipe is an ''inner'' scintillation hodoscope array segmented in azimuth into 40 (forward) and 20 (barrel) components. These are used in conjunction with a triple-layer ''outer'' hodoscope (144 total elements) [27] to form multiplicity patterns for use in the trigger. In the reaction $\bar{p}p \rightarrow 4K^{\pm}$ at least three charged tracks are required within a forward 45° cone around the beam axis. The fourth kaon has a maximum polar angle of 60°. The inner scintillator array extends to this angle, while the barrel outer array includes angles up to 135° to veto events with large angle tracks.

Between these scintillator arrays are cylindrical drift chambers (''straws'') which are used for tracking [28]. They are arranged in 12 planes with alternating horizontal and vertical orientation in the forward region. In the barrel, 1400 straws are formed into a tightly packed bundle aligned with and surrounding the beam pipe.

Three separate devices are incorporated with the purpose of providing PID information. These include 3500 silicon-pad counters which measure energy loss. They are particularly effective at the low end of the expected β range. A hodoscope consisting of 24 forward and 24 barrel threshold Čerenkov counters is positioned just inside of the outer scintillator array. These counters are used to limit the number of ''fast'' particles that are accepted at the trigger level (typically $\leqslant 2$) and, for those events which induce light in the Čerenkov counters, as a measure of the β of that passing particle. Finally, a ring-imaging Čerenkov counter (RICH) detector, having a quartz radiator ($\beta_{th}=0.64$), was introduced into the forward detector compartment following the first year of data taking [29]. It is capable of providing a precise measurement of the β for typically one of the forward-going tracks in each event. Outside of all of these components an electromagnetic calorimeter made from lead and scintillating fibers (Pb/SciFi) is placed. In the forward region the shower counter is divided into 300 towers. Each tower is 12.5 radiation lengths thick and has individual phototube readout [30]. In the barrel, 24 trapezoidal bars of Pb/SciFi form a hermetic cylinder with six radiation lengths thickness at normal incidence. The barrel calorimeter, in conjunction with the outer barrel scintillator array, has a special electronic pattern unit enabling the fast identification of isolated high-energy photons. The forward calorimeter is passive, used only in the offline analysis for evidence of high-energy gammas in the event.

The online trigger was based on a charged-particle multiplicity of four (with no more than one track in the barrel region) coupled with a crude transverse momentum balance requirement based on the forward straws multiplicity. Events with more than two of the threshold Čerenkov counters responding or with high-energy gammas in the barrel calorimeter were vetoed. These trigger conditions were tested using special runs in which such conditions were relaxed in order to determine the sensitivity of the detector acceptance to the trigger. For events meeting the trigger conditions, information was recorded from multiple parallel VME-based subsystems onto a common data stream [31] which was recorded on magnetic tape. Approximately 500 million events were recorded in eight running periods spanning the time from April 1991 through September 1994.

III. DATA SELECTION

A. Event reconstruction

The offline analysis proceeds as follows. Since the detector is non-magnetic, only the directions of the four outgoing particles in the reaction

$$\bar{p}p \rightarrow K^+K^-K^+K^- \tag{2}$$

are measured. The four momenta therefore are obtained by solving the four equations of energy-momentum conservation.

The conservation of three-momentum from the well-defined initial state (e.g., $\Delta p/p \approx 10^{-3}$ for the antiproton) allows the magnitudes of the momenta for the four kaons in the final state to be expressed as linear functions of one unknown parameter, which can be taken to be the momentum, p_4, of the fourth kaon. The total energy in the laboratory of the final state $E=\Sigma\sqrt{p_i^2+m_K^2}$ can then be written as a function of this one parameter p_4. The function $E(p_4)$ has a roughly hyperbolic shape that diverges as $p_4 \rightarrow \pm\infty$ and possesses a single minimum. We define $\Delta E = E(p_4) - E_0$ as the minimum of the function $E(p_4)$ minus the total energy E_0 of the initial state in the laboratory system. This variable ΔE is constrained to $\Delta E < 0$ for events from reaction (1), with a singularity appearing in the available phase-space at $\Delta E = 0$. The width of this spike is determined mainly by the resolution of the straw chamber tracking system which is well studied. The resulting resolution on the momentum determination is 8% at a typical kaon momentum of 0.5 GeV/c.

A Monte Carlo simulation of pure $\bar{p}p \rightarrow 4K^{\pm}$ events, with the experimental resolution and all other material effects included, results in a ΔE distribution as shown in Fig. 2(a).

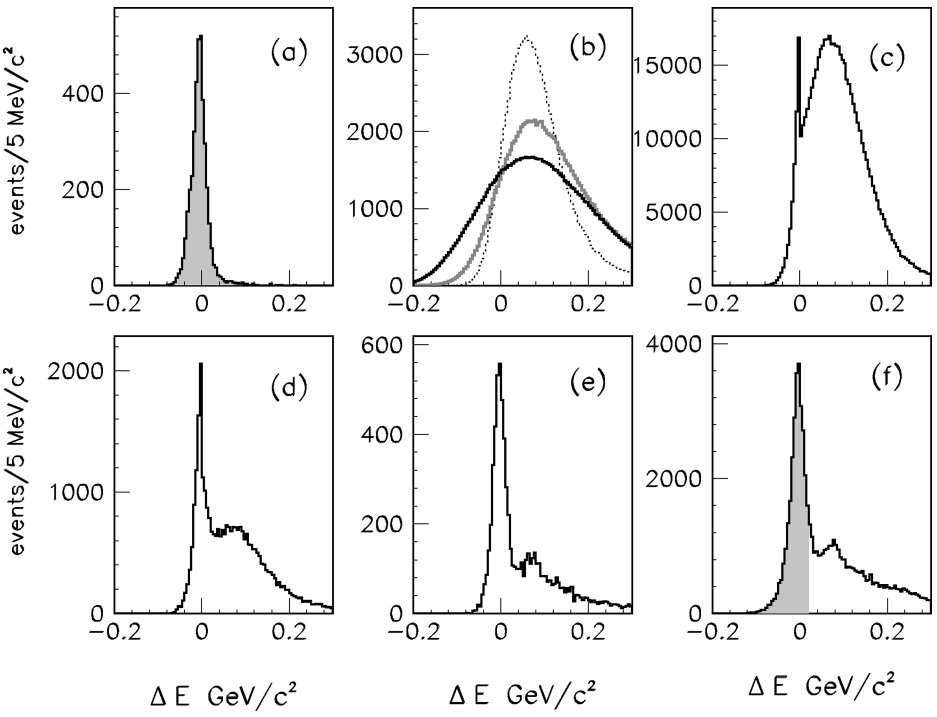

FIG. 2. ΔE (see text) distributions for (a) Monte Carlo simulation of the reaction $\bar{p}p \to 4K^{\pm}$ at 1.5 GeV/c; (b) Raw four-prong data for different momenta ranges: Light line: 1.2 GeV/c, gray line: 1.65 GeV/c, black line: 2.0 GeV/c; (c) Application of the dE/dx criterion only to data in the 1.4–1.45 GeV/c region; (d) Adding the threshold Čerenkov compatibility condition to this data; (e) Adding the criterion from the RICH and from the γ veto; (f) Final ΔE distribution for all the data taken in the experiment. The shaded area shows the cut used to select the reaction.

The distribution is asymmetric, and its width increases with increasing incident $\bar{p}$ momentum.

The four-prong data, prior to application of any PID information, show a broad ΔE distribution with no obvious structure. This is consistent with expectations since these events are dominated by background. The shape variation of such raw ΔE distributions over the span of incident momenta explored by our experiment is shown in Fig. 2(b).

B. Particle identification

In order to isolate the $\bar{p}p \to 4K^{\pm}$ events from the very large background, use of different selection criteria based on the particle identification devices is made. First we require an energy loss (dE/dx) compatibility as measured in the silicon detectors. This is evaluated by forming a confidence level for each measurement, using a parametrization of the Landau distribution and integrating the tail beyond the measured value. The confidence levels for each measurement are then combined into a dE/dx confidence level. The detectors were calibrated using a sample of well-defined tracks with known momenta. They come from fully identified $\bar{p}p$ elastic scattering events and from $\bar{p}p \to \bar{p}p\pi^+\pi^-$ events. This latter reaction was isolated almost background free by making use of the Čerenkov identification and by the requirement of a large energy deposit from the outgoing $\bar{p}$ in the forward electromagnetic calorimeter [32]. A plot of the pulse height in the silicon pads vs β is shown in Fig. 3(a) for the barrel region and in Fig. 3(b) for the forward region. The first plot makes use of elastic events, while the second distribution has been obtained from $\bar{p}p \to \bar{p}p\pi^+\pi^-$ data. Application of the dE/dx compatibility requirement on a sample of the 1.4 to 1.45 GeV/c data results in a ΔE distribution as shown in Fig. 2(c). At this stage the $\bar{p}p \to 4K^{\pm}$ events are already in evidence.

The Čerenkov effect produces a response $R(\beta)$ in photoelectrons that is monotonically increasing for $\beta \geqslant \beta_{th}$. Two different radiators were used: liquid freon (FC72) [33], in the very first data taking only, having a threshold at $\beta = 0.79$, and subsequently water having a threshold at 0.75. The result of the β measurement from the Čerenkov response events of the water radiator is compared in Fig. 4(a) to the expected β from elastic events.

For the freon data, we show in Fig. 4(b) the ''efficiency'' versus β, where we have defined efficiency as the ratio between the β distribution of the tracks crossing the Čerenkov counters which give light to the β distribution of all the tracks. This study is based on events of the type $\bar{p}p \to \bar{p}p\pi^+\pi^-$. A smooth increase as a function of β is seen which indicates the expected threshold behavior. The nonzero efficiency below threshold is caused by light produced in the plexiglass containment wall of the counters.

The response function of the liquid Čerenkov counters is used to calculate the expected signal from a passing track of a given hypothesized momentum. The expected and measured responses are compared on the basis of Poisson statistics. The resulting confidence levels for the four tracks are then combined with the one obtained from the dE/dx information to form an overall particle identification confidence level which is required to be at least 5%. The effect of add-

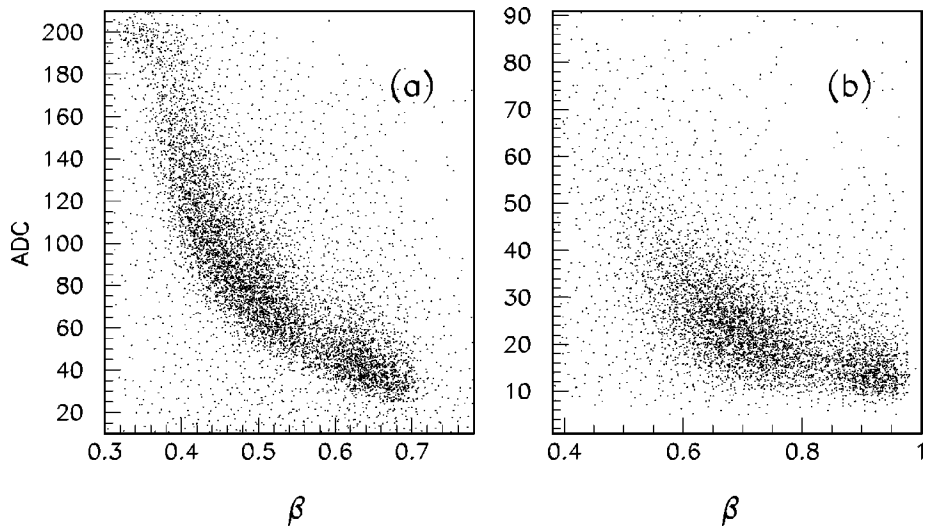

FIG. 3. (a) Pulse height in analog to digital converter (ADC) units for the barrel silicon pads vs β for a sample of elastic $\bar{p}p$ events. (b) Pulse height in ADC units for the forward silicon pads vs β from a sample of p or $\bar{p}$ from the reaction $\bar{p}p \to \bar{p}p\pi^+\pi^-$.

ing the Čerenkov information can be seen in Fig. 2(d).

The response function of the RICH is determined by measurements of elastic events in which the forward-scattered antiproton of known momentum penetrates the detector. Details of this detector performance are found elsewhere [29], however, a representative example of the β resolution is shown in Fig. 5. The difference between the expected and measured β distribution exhibits a Gaussian behavior with a resolution of $\Delta\beta/\beta \approx 2\%$. In analyzing the response of the detector, we find that a large fraction of background events produces a RICH β measurement which is unphysically greater than 1. The most effective cut eliminates this background, yet retains the good events, by simply requiring that the β measured by the RICH be less than 0.9.

One background reaction which frequently satisfies the trigger conditions of the experiment is

$$\bar{p}p \to \bar{p}p\pi^+\pi^- \tag{3}$$

which is particularly important for $\bar{p}$ momenta above 1.6 GeV/c. Reaction (3) is identified by the same selection criteria as those applied to find $\bar{p}p \to 4K^{\pm}$ events. Events so identified are removed from the final $4K^{\pm}$ sample.

At the final stage of event selection, those events with isolated γ's in the barrel region are removed. This eliminates most of the events with multiple γ's or π^0's. The final ΔE distribution after applying all the above selection criteria is shown in Fig. 2(e) for the 1.4 to 1.45 GeV/c sample and in Fig. 2(f) for all of the data taken in the experiment combined. A clear signal, peaked at a ΔE of zero, is seen which is evidence for events of the type $\bar{p}p \to 4K^{\pm}$. The final selection of events is made by requiring $\Delta E \leqslant 20$ MeV. This cut selects approximately 32 000 events which are retained for further study.

IV. ACCEPTANCE AND LUMINOSITY

The experiment accumulated data at 58 incident $\bar{p}$ momentum settings with different luminosities over a period of

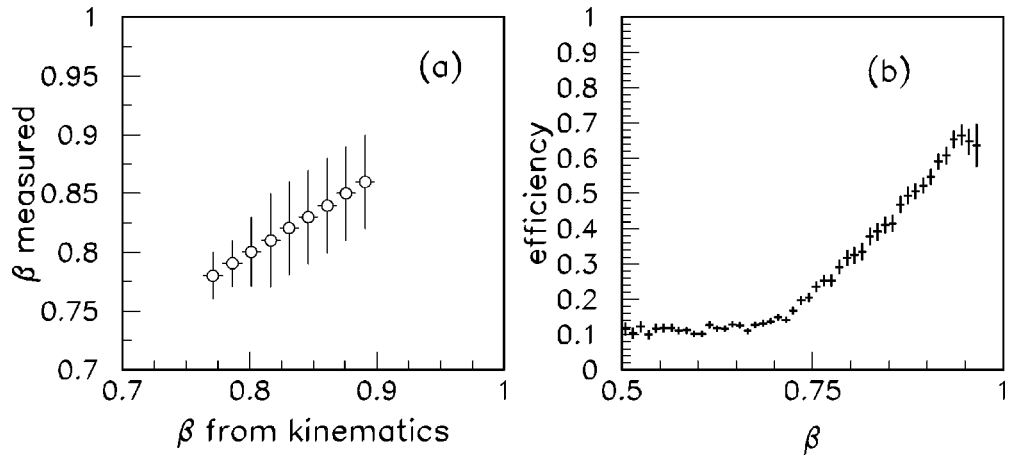

FIG. 4. (a) Measured versus expected β for elastic events in the forward Čerenkov counters with the water radiator. (b) The fraction of tracks giving light in the Čerenkovs as a function of β for the freon radiator. Events of the type $\bar{p}p \to \bar{p}p\pi^+\pi^-$ are used. Light observed below threshold results from the plexiglass walls of the counters.

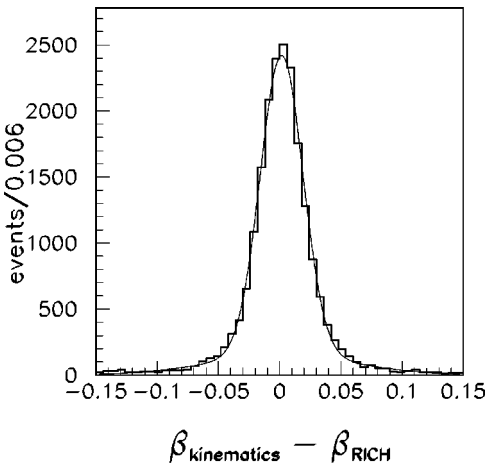

FIG. 5. Expected minus measured β from the RICH detector for elastic events.

four years. However, in the following analysis, measurements at the same or nearly the same momentum have been grouped together in order to reduce statistical and systematic errors. The distribution of luminosities as a function of the momentum are summarized in Table I.

The luminosity was monitored via the known cross section of elastic $\bar{p}p$ scattering. Two independent methods were employed to measure it. In the first method, the rate of coincidence between opposite pixels formed in the outer trigger scintillator hodoscope was used to count elastic events near 90° in the c.m. system. The second method made use of small microstrip detectors placed near 90° in the barrel to detect the recoil particle from low-angle elastic scattering [34]. The data have been normalized as a function of time by using minimum bias scalers which were found to be very reliable and stable over the lifetime of the experiment. The relative luminosity error is 2%.

The acceptance for the elastic and $4K$ events was computed by a GEANT [35] based Monte Carlo simulation of the physical detector and trigger conditions. The Monte Carlo events were subjected to the same reconstruction criteria and analysis cuts as the real data. We generated Monte Carlo events for each of the 58 momentum settings, taking into account the changes in the layout of the apparatus and trigger conditions. For the physics analysis, three reactions were generated: $\bar{p}p \to \phi\phi$, $\bar{p}p \to \phi K^+K^-$ and $\bar{p}p \to K^+K^-K^+K^-$. The simulation assumed phase space distributions for all three reactions. The distributions of the total acceptance as a function of the incident $\bar{p}$ momentum are shown as fitted polynomials in Fig. 6(a).

The differential acceptance function for $\bar{p}p \to \phi\phi$ is greatly affected by the kinematics of the reaction and the layout of the detector. The distribution of $\cos\Theta_{cm}$ is shown in Fig. 6(b) for all the data. Here, Θ_{cm} is defined as the center-of-mass scattering angle of the outgoing ϕ. A strong depletion of events occurs in the forward region, due to loss of tracks in the beam pipe. On the other hand, the acceptance in the χ angle is almost flat as it can be seen in Fig. 6(c). Here χ is defined as the angle formed by the two ϕ's decay planes, in the $\phi\phi$ center of mass system. Figure 6(c) shows the distribution of the χ angle for the data in the 1.26–1.65 GeV/c region (points with error bars), together

TABLE I. Cross sections for $\bar{p}p \to \phi\phi$, ϕK^+K^- and $4K$.

Momentum region GeV/c	c.m. energy GeV/c^2	Luminosity nb^{-1}	$\sigma(\phi\phi)$ μb	$\sigma(\phi K^+K^-)$ μb	c.m. energy GeV/c^2	$\sigma(4K^{\pm})$ μb
1.188–1.200	2.147	26.8	2.86±0.46	0.25±0.49	2.158	0.15±0.15
1.237–1.278	2.168	32.8	3.45±0.31	0.96±0.32		
1.300–1.330	2.190	69.1	3.54±0.18	0.23±0.21	2.195	0.56±0.13
1.360	2.205	33.4	3.84±0.24	0.27±0.26		
1.390–1.400	2.218	60.7	3.55±0.17	0.63±0.22	2.219	0.50±0.17
1.404–1.405	2.220	53.9	3.88±0.17	0.54±0.21		
1.410–1.415	2.223	38.0	4.00±0.20	0.39±0.25	2.225	0.52±0.15
1.420	2.226	25.7	3.84±0.24	0.71±0.29		
1.425–1.430	2.228	26.4	3.09±0.22	0.97±0.32		
1.435	2.231	47.7	3.33±0.17	1.16±0.235	2.233	0.58±0.15
1.440–1.450	2.235	35.1	3.41±0.19	1.19±0.26		
1.465–1.480	2.242	48.7	3.02±0.15	1.07±0.22	2.247	0.44±0.26
1.500–1.506	2.255	42.7	3.01±0.16	1.77±0.25		
1.550	2.272	24.3	2.25±0.17	1.90±0.31	2.282	0.34±0.33
1.600	2.289	20.1	2.15±0.21	2.40±0.40		
1.650	2.307	13.6	1.97±0.24	3.26±0.45		
1.700–1.750	2.333	32.6	2.04±0.14	3.56±0.30	2.348	0.95±0.52
1.800	2.360	39.3	2.04±0.12	4.30±0.25		
1.900–1.950	2.404	15.4	1.61±0.18	3.63±0.41	2.424	2.55±0.93
2.000	2.430	52.1	1.93±0.11	3.91±0.24		

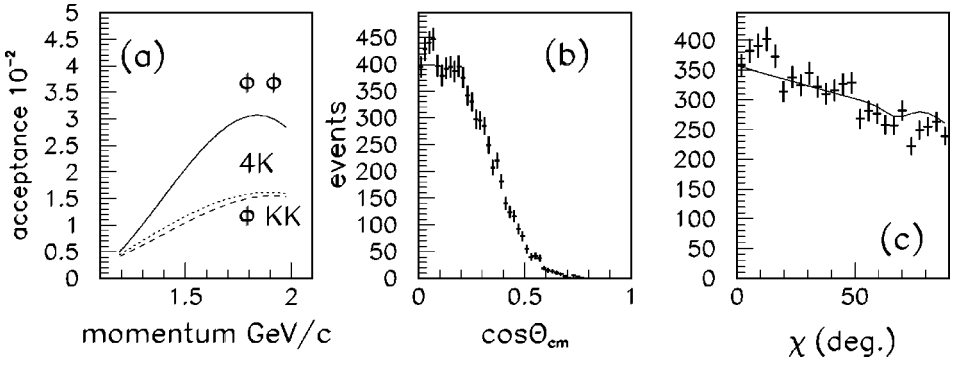

FIG. 6. (a) Acceptance for the three reactions $\bar{p}p \to \phi\phi$, $\bar{p}p \to \phi K^+K^-$ and $\bar{p}p \to 4K^{\pm}$. Distribution of (b) $\cos\Theta_{cm}$ and (c) χ for the reaction $\bar{p}p \to \phi\phi$ in the momentum range between 1.26 and 1.65 GeV/c. The data are represented with error bars. In (c) the solid line represents the distribution expected for phase space.

with the distribution of χ for Monte Carlo phase space generated data folded with the acceptance of the apparatus. This missing forward angle acceptance in Θ_{cm} affects our ability to extract total $\phi\phi$ cross sections as described later.

Systematic errors on the cross section measurements have been estimated using the known cross section for $\bar{p}p \to \bar{p}p\pi^+\pi^-$ [32] whose determination was found to be in good agreement with previous measurements. We also used the fact that the cross sections at several energy points were measured several times under different experimental conditions. We estimate the overall uncertainty on the absolute scale of the $\phi\phi$ cross section to be 20%.

V. THE DATA

For the selected $\bar{p}p \to K^+K^-K^+K^-$ event candidates we show in Fig. 7, in Fig. 8(a) and in Fig. 8(b) the scatter plot of the invariant masses $m(K_3K_4)$ vs $m(K_1K_2)$. Figure 7 shows all the available data as a surface plot, where a strong accumulation of events can be observed at the nominal $\phi\phi$ position. Figure 8(a) and 8(b) illustrate the same data under the form of a scatter diagram for two different regions of incident $\bar{p}$ momentum, i.e. below and above 1.5 GeV/c, respectively. Notice that, due to the absence of charge information, three combinations per event enter in these plots. We observe in these distributions a strong enhancement at the position of the $\phi\phi$. In the higher momentum region we also observe horizontal and vertical bands which indicate the presence of the $\bar{p}p \to \phi K^+K^-$ final state. Monte Carlo simulations confirm that the diagonal bands represent the reflection of the $\phi\phi$ peak due to the multiple combinations. Selecting one ϕ, i.e. requiring one $m(K_3K_4)$ combination to lie in the region 1.00–1.04 GeV/c^2 and plotting the opposite combination $m(K_1K_2)$, we obtain the distributions shown in Fig. 8(c) and 8(d), where a clean ϕ peak is visible. The structure is well centered at the nominal ϕ mass.

VI. CHANNEL LIKELIHOOD FIT

In order to separate the $\phi\phi$ cross section from the ϕK^+K^- final state and from the $4K$ and other background mixture, the channel likelihood technique [36] was used. The method performs a maximum likelihood fit to the data using three amplitudes: $\phi\phi$, ϕK^+K^- and phase space (which is a mixture of $4K$ and background and cannot be separated at this stage). The different channels have been described by the following amplitudes:

$$\phi\phi: A_{\phi\phi} = \sum_{i,j=1}^{3} B_i(m_{KK}) \times B_j(m_{KK})$$

$$\phi KK: A_{\phi KK} = \sum_{i=1}^{6} B_i(m_{KK}).$$

The likelihood function employed is the following:

$$\mathcal{L} = x_{\phi\phi}\frac{A_{\phi\phi}}{I_{\phi\phi}} + x_{\phi KK}\frac{A_{\phi KK}}{I_{\phi KK}} + (1 - x_{\phi\phi} - x_{\phi KK}).$$

In the above expressions $x_{\phi\phi}$ and $x_{\phi KK}$ represent the fractions of the $\phi\phi$ and ϕK^+K^- channels, respectively, $B_i(m_{KK})$ represents the ϕ line shape functions, $I_{\phi\phi}$ and $I_{\phi KK}$

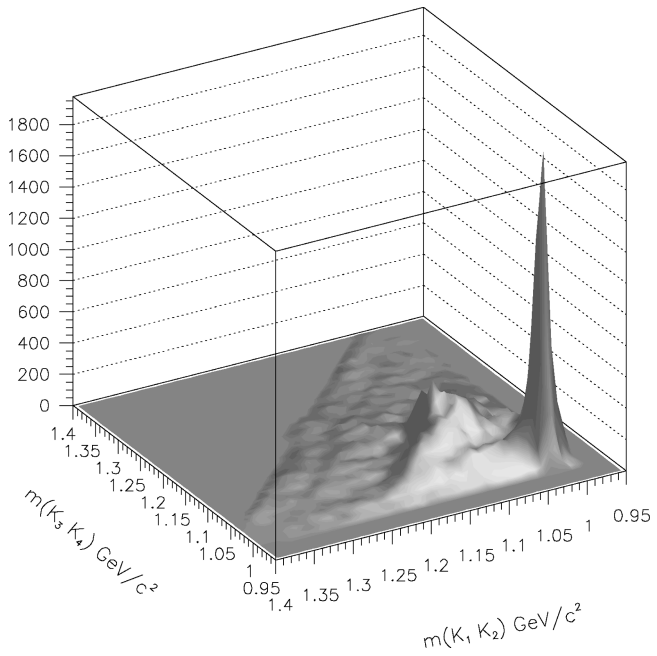

FIG. 7. $m(K_3,K_4)$ vs $m(K_1,K_2)$ (three combinations per event) for all the events.

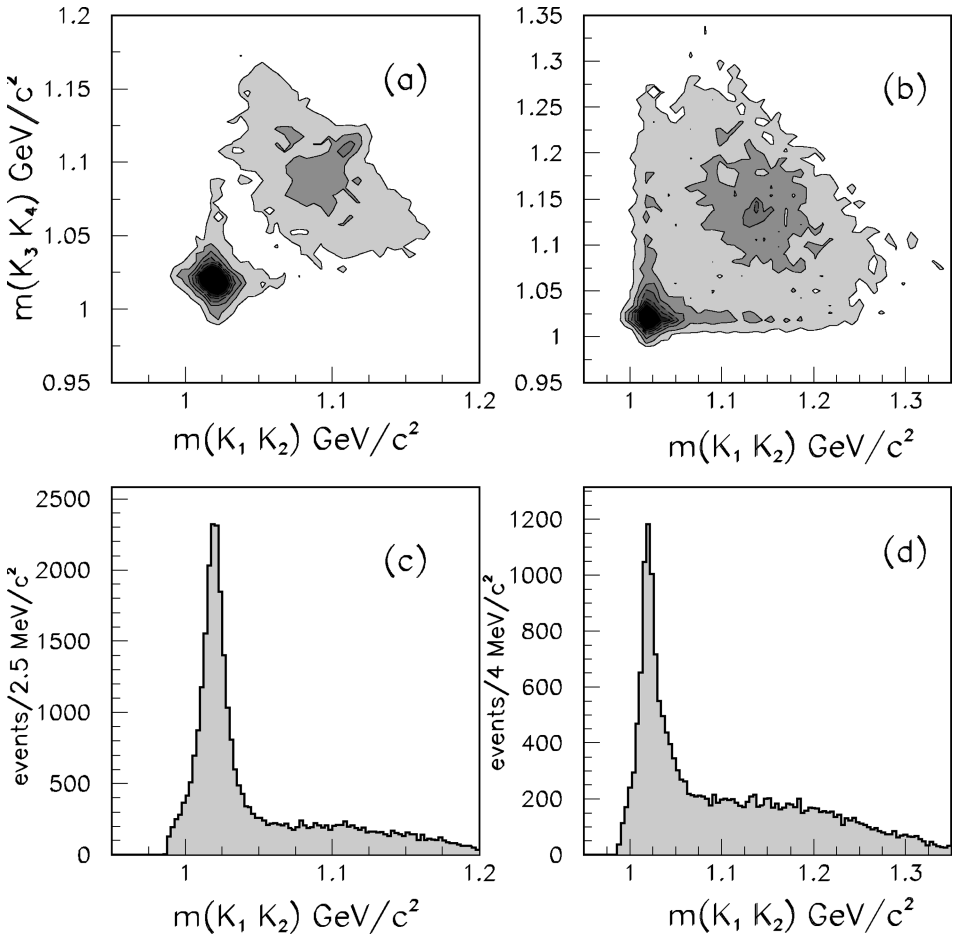

FIG. 8. $m(K_3,K_4)$ vs $m(K_1,K_2)$ (three combinations per event) for (a) $\bar{p}$ incident momentum below 1.5 GeV/c and (b) above 1.5 GeV/c. (c), (d) mass projections of (a) and (b) in the ϕ band, i.e. plots of $m(K_1K_2)$ for $1.00 \leqslant m(K_3,K_4) \leqslant 1.04$ GeV/c^2.

represent the corresponding normalization integrals for the two amplitudes describing the two channels, respectively.

The ϕ width is a narrow resonance ($\Gamma = 4.4$ MeV), therefore, the observed width in this experiment is dominated by the detector resolution which we found to be non-Gaussian. In order to describe the ϕ line shape, we made use of the Monte Carlo simulations. The best representation of this line shape is obtained by means of a relativistic spin 0 Breit-Wigner form whose full width varies from 11 to 15 MeV as the incident $\bar{p}$ momentum increases from 1.1 to 2.0 GeV/c.

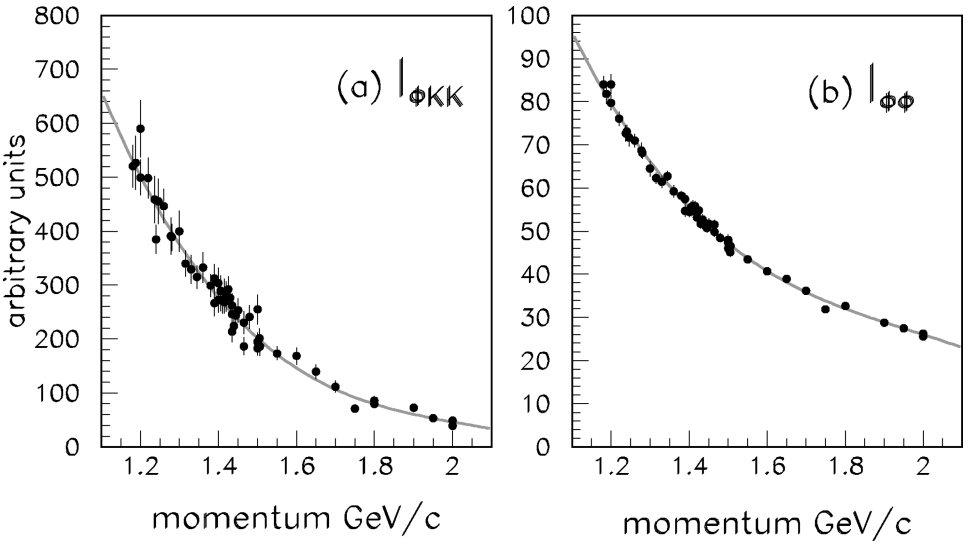

FIG. 9. Variation of the normalization integrals for the amplitudes describing the ϕK^+K^- (a) and $\phi\phi$ (b) amplitudes as functions of the incident $\bar{p}$ momentum.

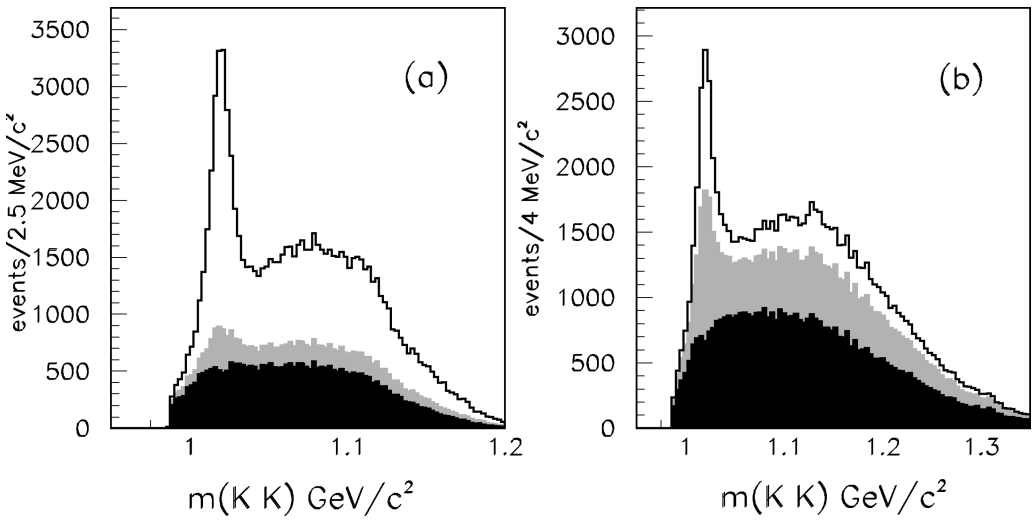

FIG. 10. Combinatorial m(KK) distribution (six entries per event) for incident $\bar{p}$ momentum (a) below and (b) above 1.5 GeV/c. The white region represents the $\phi\phi$ contribution, the gray region shows the ϕK^+K^- contribution and the black region shows the phase space (background+4K) contribution.

The normalization of the amplitudes was computed numerically using the Monte Carlo simulations of the reaction $\bar{p}p \to 4K$. The resulting integrals were then fit to polynomials as functions of the incident $\bar{p}$ momentum. Changes in the layout of the apparatus and trigger conditions have little effect on the values of these integrals as seen in Fig. 9, where these integrals and the fitted polynomials are shown.

The channel likelihood fit gives the fractions of events as well as a probability for each event to belong to one of the three hypotheses. The results of the fits are visually dis-

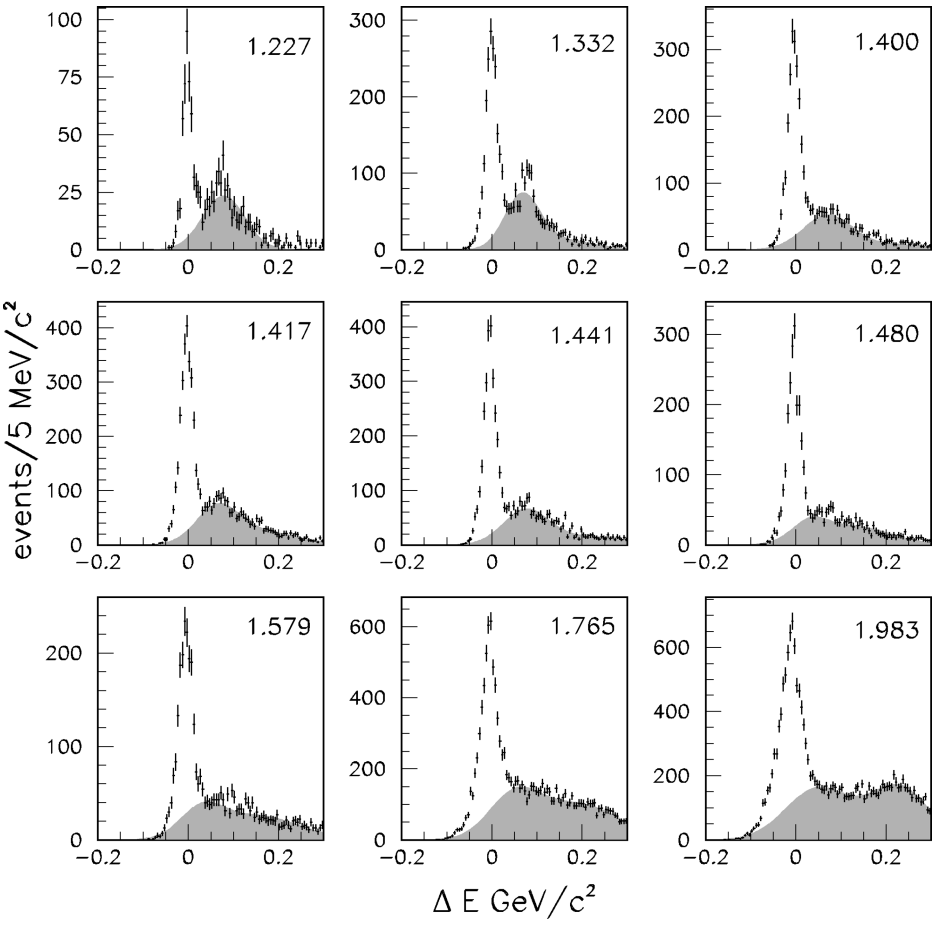

FIG. 11. ΔE distributions for the nine regions in increasing values of incident $\bar{p}$ momentum. The gray area represents the estimated background.

played in Fig. 10. Here we show the combinatorial $m(KK)$ distribution (six entries per event) for incident $\bar{p}$ momentum below and above 1.5 GeV/c. The white region represent the $\phi\phi$ contribution, the gray region shows the ϕK^+K^- contribution, while the black region shows the phase space (background+$4K$) contribution. We notice that no ϕ peak has been left in the phase space distribution, indicative of a successful fit. We also notice the strong increase of the ϕK^+K^- contribution in the higher momentum region. The analysis gives a total of approximately 11 400 $\phi\phi$ events.

The channel likelihood method is able to separate the three $\phi\phi$, ϕK^+K^- and (background+$4K$) contributions. In order to separate the $4K$ contribution from the background, we made use of the ΔE distributions as discussed in Sec. III A. For this purpose, in order to reduce the errors, a further compression of the data was performed, grouping them in nine slices of incident $\bar{p}$ momentum. The ΔE distributions for all intervals are shown in Fig. 11. A clean peak at $\Delta E = 0$ over some background is observed which represents the total amount of the reaction $\bar{p}p \to 4K$ including $\phi\phi$ and ϕK^+K^- contributions. These distributions have been fitted using a Monte Carlo generated shape for the ΔE distribution which includes simulations at all energies of $\phi\phi$ and $4K$ final states, and a background parametrization using the sum of two Gaussians. The number of non-resonant $4K$ events was therefore obtained by

$$N_{4K} = N_T - N_{\phi\phi} - N_{\phi KK} - N_b .$$

In the above expression, the number of $4K$ events is the difference between the total number of events in each bin (N_T), the $\phi\phi$ ($N_{\phi\phi}$) and ϕK^+K^- ($N_{\phi KK}$) yields which were obtained from the channel likelihood fits, and the background (N_b) is drawn from the fits to the ΔE distributions. Due to the uncertainty in the background subtraction, a 50% systematic error has been added quadratically to the statistical errors. The background below the $4K$ signal is relatively small, being in average of the order of 10% increasing to 20% only in the higher momentum regions.

VII. CROSS SECTIONS

Having determined the number of events for each channel, we have computed the corresponding cross sections as

$$\sigma = \frac{\text{events}}{\text{acceptance} \times \text{luminosity}}.$$

Due to decreasing performance of the threshold Čerenkov counters in the last period of the data taking, part of data suffer an additional 20% systematic normalization error. These data represent about 30% of the total and have not been used in the calculation of the cross sections. However, properly scaled, these data can be used in the study of the angular distributions. These cross sections have been corrected for unseen ϕ decay modes and are displayed in Table I and shown in Fig. 12.

The $\phi\phi$ cross section has been corrected assuming phase space in the calculation of the acceptance. This is not really a strong assumption as it can be seen from Fig. 6(c). In addition, a spin parity analysis of the $\phi\phi$ final state has been performed [37]. This analysis shows that the $\phi\phi$ system is dominated by $J^{PC} = 2^{++}$. Correcting the mass spectrum with the results from the spin-parity analysis has little influence on the shape of the integrated acceptance as a function of the $\phi\phi$ mass.

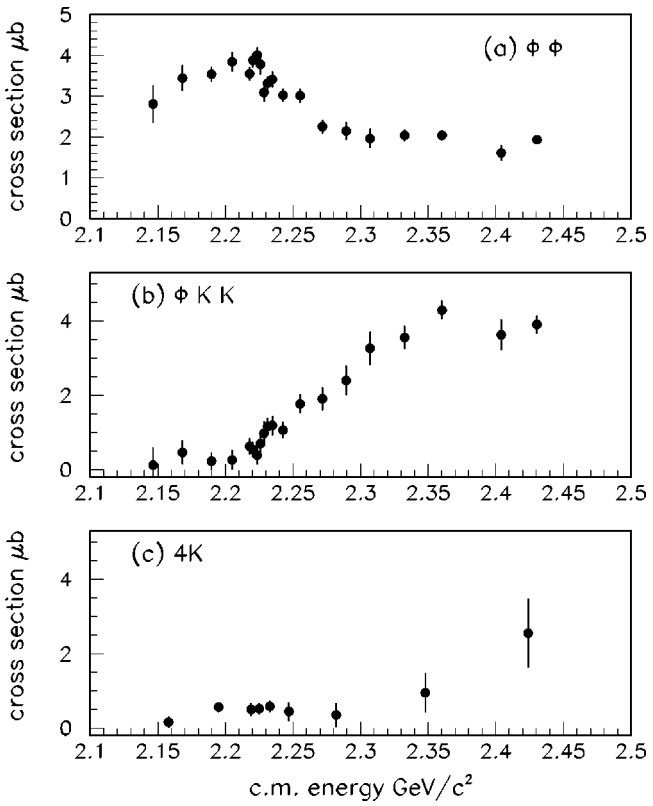

FIG. 12. Cross sections in μb for the reactions (a) $\bar{p}p \to \phi\phi$, (b) $\bar{p}p \to \phi K^+K^-$ and (c) $\bar{p}p \to 2K^+2K^-$ corrected for unseen ϕ decay modes.

Notice that:

The $\phi\phi$, ϕK^+K^- and $4K^{\pm}$ cross sections have different shapes. The $\phi\phi$ cross section, in particular, has a strong threshold enhancement, while the ϕK^+K^- and $4K^{\pm}$ cross sections have a smooth increase as a function of the center of mass energy.

The $\phi\phi$ cross section is rather large, about 3.5 μb in the threshold region.

No evidence for narrow structures is found.

The large $\phi\phi$ production close to threshold can be interpreted as a violation of the (OZI) rule. If the OZI rule is interpreted to forbid strangeness production in $\bar{p}p$ annihilations then the process $\bar{p}p \to \phi\phi$ can proceed only via the small $\bar{u}u, \bar{d}d$ component present in the ϕ wave function. With a deviation from ideal mixing $\theta - \theta_0$ of only 1^0 to 4^0, the ϕ is nearly 100% $\bar{s}s$. We can therefore derive an upper limit $\tan^4(\theta - \theta_0) \approx 2.5 \times 10^{-5}$ for the ratio of cross sections $\sigma_{\phi\phi}/\sigma_{\omega\omega}$ for production in $\bar{p}p$ annihilation. Although the cross section of $\bar{p}p \to \omega\omega$ has not been measured directly, an estimate can be obtained from the total $2\pi^+2\pi^-2\pi^0$ cross section [38], which was measured to be about 5 mb in the energy range of our experiment. There are many reaction channels that contribute to this final state. If we estimate that

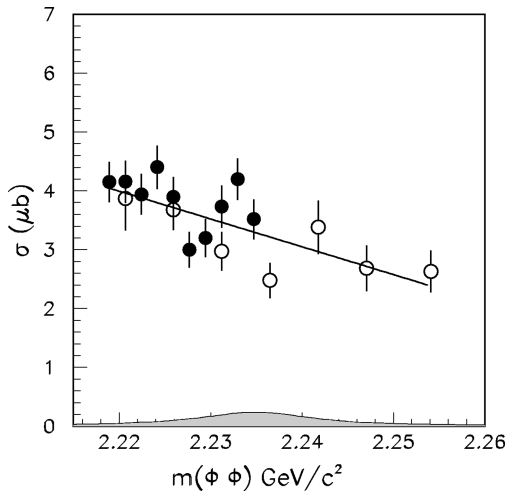

FIG. 13. Cross section in μb for the reaction $\bar{p}p \to \phi\phi$ in a fine scan over two different periods of data collection corrected for unseen ϕ decay modes. Open circles: 1991 data; full circles: 1993 data. The line is the result from the fit described in the text, the curve represents a Breit-Wigner resonance whose amplitude is at the 95% c.l. upper limit for the production of a $\xi/f_J(2230)$ with a mass of 2235 MeV and a width of 15 MeV.

it is 10% $\omega\omega$, then the expected $\phi\phi$ cross section is 10 nb, two orders of magnitude lower than our measurements.

VIII. SEARCH FOR $\xi/f_J(2230)$

To search for the $\xi/f_J(2230)$ resonance, a fine scan of the $\phi\phi$ cross section was performed during two different data taking periods. The results from these scans are shown in Fig. 13 and displayed in Table II.

Here the empty and full dots distinguish the two different sets of the data, showing good agreement in the size of the $\phi\phi$ cross section. No narrow structure is visible in the data. We have fitted the $\phi\phi$ mass spectrum using a polynomial and a Breit-Wigner form representing the $\xi/f_J(2230)$ with m=2235 MeV and $\Gamma = 15$ MeV, parameters measured in the reaction $J/\psi \to \gamma\xi$ where $\xi \to \bar{p}p$ by the Beijing Spectrometer (BES) experiment [19]. The Breit-Wigner form is written as:

$$\sigma_{BW} = (w_i w_f)\,\frac{(2J+1)}{(2S_1+1)(2S_2+1)}\,\frac{4\pi(\hbar c)^2}{s-4m_p^2} \times \frac{\Gamma^2}{(\sqrt{s}-m_{res})^2+\Gamma^2/4}. \quad (4)$$

Here $(w_i w_f)$ is the double branching ratio, $w_i w_f = \mathrm{B}(X \to \bar{p}p) \times \mathrm{B}(X \to \phi\phi)$. The S_i terms are the spins of the initial proton and antiproton (1/2), and J is the total angular momentum of the resonance, reducing the angular momentum term, $(2J+1)/[(2S_1+1)(2S_2+1)]$ to 5/4 in the case of a $J=2$ resonance. A limit on the product of the branching ratios of $\mathrm{B}(\xi \to \bar{p}p) \times \mathrm{B}(\xi \to \phi\phi) \leqslant 6 \times 10^{-5}$ at 95% c.l. is obtained.

TABLE II. $\phi\phi$ cross section for the fine scan.

c.m. energy GeV/c^2	$\sigma(\phi\phi)$ μb
2.219	4.15±0.34
2.221	4.16±0.36
2.221	3.87±0.54
2.222	3.94±0.35
2.224	4.40±0.36
2.226	3.90±0.34
2.226	3.68±0.34
2.228	3.00±0.30
2.229	3.20±0.32
2.231	3.73±0.35
2.231	2.97±0.33
2.233	4.20±0.35
2.235	3.52±0.34
2.236	2.48±0.30
2.242	3.38±0.45
2.247	2.68±0.39
2.254	2.63±0.35

IX. CONCLUSIONS

We have performed a high statistics study of the reaction $\bar{p}p \to 4K^{\pm}$ using in-flight $\bar{p}$ from 1.1 to 2.0 GeV/c incident momentum interacting on a hydrogen jet target of the JETSET (PS202) experiment at CERN LEAR. The reaction is dominated by a strong $\phi\phi$ production at threshold whose strength exceeds by two orders of magnitude the yield extracted from a simple interpretation of the OZI rule.

Several models have been proposed in order to explain the large OZI violations observed in hadron induced reactions and particularly in some $\bar{p}p$ annihilation channels. However, few quantitative calculations exist for the specific channel under investigation in the present experiment.

A model which interprets $\bar{p}p$ annihilations to $\phi\phi$ as due to $K\bar{K}$ rescattering [39] is able to predict the order of magnitude of the cross section (≈ 2.4 μb), but not the detailed shape of the observed spectrum. Other models make use of hyperon-antihyperon intermediate states [10]. In this case the size of the cross section is underestimated by a factor of about 4. Other ways to enhance production of the $\phi\phi$ system have been suggested in Ref. [12] by invoking the hypothesis of intrinsic strangeness content in the proton. The authors suggest that $\phi\phi$ production could originate from rearrangement diagrams with strange quarks originating from the proton sea which are polarized with total spin S=1. The authors conclude that these connected rearrangement diagrams very likely mask any possible glueball resonance contributions which are expected to be dominant among the disconnected diagrams. Further information and possible new inputs to the problem may come from a spin analysis of the observed $\phi\phi$ threshold enhancement [37].

No evidence for narrow resonance is found and we set an upper limit for the production of $\xi/f_J(2230)$ with m=2235 MeV and $\Gamma = 15$ MeV of: $\mathrm{B}(\xi \to \bar{p}p) \times \mathrm{B}(\xi \to \phi\phi) \leqslant 6 \times 10^{-5}$ at 95% c.l. Combined with our scan of $\bar{p}p \to K_S^0 K_S^0$ [20] a consistent and stringent rejection of a narrow resonance ($\Gamma < 30$ MeV) appears.

ACKNOWLEDGMENTS

We thank the teams of the CERN Antiproton Complex, in particular the LEAR staff. This work has been supported in part by CERN, the German Bundesministerium für Bildung, Wissenschaft, Forschung und Technologie, the Italian Istituto Nazionale di Fisica Nucleare, the Swedish Natural Science Research Council, the Norwegian Research Council, and the United States National Science Foundation.

[1] G. S. Bali *et al.*, Phys. Lett. B **309**, 378 (1993); J. Sexton, A. Vacarino and D. Weingarten, Phys. Rev. Lett. **75**, 4563 (1995).
[2] See for example, A. Ostrovidov, Proceedings of Hadron '97 Upton, New York, 1997, AIP Conf. Proc. (AIP, New York, 1998); D. I. Ryabchikov, *Proceedings of Hadron 95*, Manchester, UK (World Scientific, Singapore, 1996); J. Dowd, *Proceedings of Hadron 91*, University of Maryland, College Park (World Scientific, Singapore, 1992).
[3] L. Kopke and N. Wermes, Phys. Rep. **174**, 67 (1989).
[4] A. Palano, *Proceedings of the IX Workshop on Photon-Photon Collisions*, San Diego, 1992 (World Scientific, Singapore, 1992), p. 308.
[5] H. Kolanoski, *Proceedings of the IX Workshop on Photon-Photon Collisions*, San Diego, 1992 (World Scientific, Singapore, 1992), p. 3.
[6] C. Amsler, ''Proton-Antiproton Annihilation and Meson Spectroscopy with the Crystal Barrel,'' hep-ex/9708025, 1997.
[7] S. Okubo, Phys. Lett. **5**, 165 (1963); G. Zweig, CERN Report No. TH-412, 1964; J. Iizuka, Prog. Theor. Phys. Suppl. **37/38**, 21 (1966).
[8] L. Bertolotto *et al.*, Phys. Lett. B **345**, 325 (1995).
[9] H. Lipkin, Phys. Lett. **124B**, 509 (1983).
[10] V. Mull, The $\bar{N}N \to \pi\pi$ and $\bar{N}N \to \phi\phi$ reactions with hadronic models, presented at NAN'93, Moscow, Russia, 1993; V. Mull *et al.*, Report. No. KFA-IKP(TH)-1994-27.
[11] S. J. Lindenbaum, Comments Nucl. Part. Phys. **13**, 285 (1984).
[12] J. Ellis *et al.*, Phys. Lett. B **353**, 319 (1995); M. Alberg *et al.*, *ibid.* **356**, 113 (1995).
[13] C. Amsler *et al.*, Phys. Lett. B **355**, 425 (1995).
[14] C. Amsler *et al.*, Phys. Lett. B **340**, 259 (1994).
[15] A. Abele *et al.*, Phys. Lett. B **385**, 425 (1996).
[16] T. Armstrong *et al.*, Phys. Lett. B **307**, 399 (1993).
[17] C. Amsler and F. E. Close, Phys. Lett. B **353**, 385 (1995).
[18] R. M. Baltrusaitis *et al.*, Phys. Rev. Lett. **56**, 107 (1986).
[19] J. Z. Bai *et al.*, Phys. Rev. Lett. **76**, 3502 (1996).
[20] C. Evangelista *et al.*, Phys. Rev. D **56**, 3803 (1997).
[21] D. Bisello *et al.*, Phys. Lett. B **179**, 294 (1986); G. Eigen, International School of Physics with Low Energy Antiprotons, Erice, Sicily, 1987 (Plenum, New York, 1989).
[22] T. A. Armstrong *et al.*, Nucl. Phys. **B196**, 176 (1982).
[23] S. J. Lindenbaum, Phys. Lett. **131B**, 221 (1983); A. Etkin *et al.*, *ibid.* **165B**, 217 (1985); A. Etkin *et al.*, Phys. Lett. B **201**, 568 (1988).
[24] P. Booth *et al.*, Nucl. Phys. **B273**, 677 (1986).
[25] N. H. Hamann *et al.*, *Proceedings of the International School on Physics with Low-Energy Antiprotons (4th Course: Medium-Energy Antiprotons and the Quark–Gluon Structure of Hadrons)*, Erice, Sicily, 1990, edited by R. Landua, J.-M. Richard and R. Klapisch (Plenum, New York, 1991), p. 165.
[26] M. Macri, GAS Jet Internal Target in Report No. CERN 84/15 p. 469 (1984).
[27] M. Dahmen *et al.*, Nucl. Instrum. Methods Phys. Res. A **348**, 97 (1994).
[28] N. H. Hamann *et al.*, Nucl. Instrum. Methods Phys. Res. A **346**, 57 (1994).
[29] R. T. Jones *et al.*, Nucl. Instrum. Methods Phys. Res. A **343**, 208 (1994); S. Passaggio and R. T. Jones, Nucl. Instrum. Methods Phys. Res. A **371**, 188 (1996).
[30] D. W. Hertzog *et al.*, Nucl. Instrum. Methods Phys. Res. A **294**, 512 (1990).
[31] P. E. Reimer, *Meson Production Interactions and Decay*, edited by A. Magiora, W. Oelert and E. Grosse (World Scientific, Singapore, 1991), p. 292.
[32] A. Buzzo *et al.*, Z. Phys. C **76**, 475 (1997).
[33] FC72 is the trade name of a compound marked by 3M composed of C_6F_{14}, sometimes known as ''liquid freon.''
[34] S. Pomp *et al.*, Nucl. Instrum. Methods Phys. Res. A **370**, 381 (1996).
[35] R. Brun *et al.*, GEANT3, CERN Report No. DD/EE/84-1, 1987.
[36] P. E. Condon and P. Cowell, Phys. Rev. D **9**, 2558 (1974).
[37] A. Palano, *Recent Results from JETSET*, Proceedings of Hadron '95, Manchester, UK (World Scientific, 1996); A. Buzzo *et al.*, Partial Wave Analysis of the reaction $\bar{p}p \to \phi\phi$ (in preparation).
[38] P. D. Zemany *et al.*, Phys. Rev. D **23**, 1473 (1981).
[39] Y. Lu *et al.*, Z. Phys. A **345**, 207 (1993).